crystals

MDPI

Article

Hot-Corrosion and Particle Erosion Resistance of Co-Based Brazed Alloy Coatings

Ion-Dragoș Uțu [1,*], Iosif Hulka [2], Norbert Kazamer [3], Albert Titus Constantin [4] and Gabriela Mărginean [5]

[1] Department of Materials and Manufacturing Engineering, Faculty of Mechanical Engineering, Politehnica University of Timișoara, Blvd. Mihai Viteazu, 300222 Timișoara, Romania
[2] Research Institute for Renewable Energies, Politehnica University of Timișoara, G. Muzicescu 138, 300501 Timișoara, Romania; iosif.hulka@upt.ro
[3] Westphalian Energy Institute, Westphalian University of Applied Sciences Gelsenkirchen Bocholt Recklinghausen, Neidenburger Str. 43, 45897 Gelsenkirchen, Germany; norbert.kazamer@w-hs.de
[4] Department of Hydrotechnical Engineering, Civil Engineering Faculty, Politehnica University of Timișoara, Splaiul Spiru Haret 1A, 300222 Timișoara, Romania; albert.constantin@upt.ro
[5] Department of Materials Science and Testing, Westphalian University of Applied Sciences Gelsenkirchen Bocholt Recklinghausen, Neidenburger Str. 43, 45897 Gelsenkirchen, Germany; gabriela.marginean@w-hs.de
* Correspondence: dragos.utu@upt.ro; Tel.: +40-256-403656

Abstract: Tape brazing constitutes a cost-effective alternative surface protection technology for complex-shaped surfaces. The study explores the characteristics of high-temperature brazed coatings using a cobalt-based powder deposited on a stainless-steel substrate in order to protect parts subjected to hot temperatures in a wear-exposed environment. Microstructural imaging corroborated with x-ray diffraction analysis showed a complex phased structure consisting of intermetallic Cr-Ni, C-Co-W Laves type, and chromium carbide phases. The surface properties of the coatings, targeting hot corrosion behavior, erosion, wear resistance, and microhardness, were evaluated. The high-temperature corrosion test was performed for 100 h at 750 °C in a salt mixture consisting of 25 wt.% NaCl + 75 wt.% Na_2SO_4. The degree of corrosion attack was closely connected with the exposure temperature, and the degradation of the material corresponding to the mechanisms of low-temperature hot corrosion. The erosion tests were carried out using alumina particles at a 90° impingement angle. The results, correlated with the microhardness measurements, have shown that Co-based coatings exhibited approximately 40% lower material loss compared to that of the steel substrate.

Keywords: co-based alloys; hot corrosion; solid particle erosion; microstructure; brazing

Citation: Uțu, I.-D.; Hulka, I.; Kazamer, N.; Constantin, A.T.; Mărginean, G. Hot-Corrosion and Particle Erosion Resistance of Co-Based Brazed Alloy Coatings. *Crystals* **2022**, *12*, 762. https://doi.org/10.3390/cryst12060762

Academic Editor: Bolv Xiao

Received: 7 April 2022
Accepted: 24 May 2022
Published: 26 May 2022

1. Introduction

In many high-temperature applications, industrial components are exposed to different phenomena such as wear, corrosion, or oxidation. The cost of both wear and corrosion is believed to be a significant fraction of the national gross domestic products GDPs estimated from 3 to 5% and even reaching up to 10% in developing countries [1]. Although stainless steels and superalloys are known for their remarkable characteristics in such applications, they fail at covering some important aspects. For instance, stainless steels are a family of materials suitable mainly for extremely severe conditions due to the corrosion protection and high-temperature mechanical properties they provide. They are, however, less adapted to fields requiring high-wear resistance [2,3]. A solution for extending the lifespan of components which operate in corrosive environments with high-wear loads could be protective resistant coatings on high-temperature resistant stainless steels and superalloys. Usually, stainless steels are coated with superalloys for greater strength [2,4–6]. Depositing coatings is a smarter and less expensive way of meeting the industrial design requirements for such materials [6].

Nickel-based alloys are preferred in many high-temperature applications due to the attractive price of nickel. Co-based alloys are versatile and well-suited materials for coatings with excellent surface properties under high-temperature conditions [7,8]. They have good mechanical properties (especially strength at high temperature) and superior wear resistance compared to nickel-based alloys [9,10]. The alloys are described as wear, corrosion, and heat-resistant materials [11,12]. Welding and laser cladding are well-known conventional technologies used for surface refurbishment of damaged components [13]. Other technologies like thermal spraying (flame and plasma spraying, high velocity oxygen fuel spraying, cold gas spray, etc.) [14,15] and laser cladding [16,17] are used to deposit these alloys on engineering components in order to prolong their lifespan [11]. Both nickel- and cobalt-based alloys are processed nowadays using the aforementioned techniques, which contribute to partial remelting and mixing of the base material with the deposited coating. Thereby, new phases with a brittle aspect could be generated along the interface coating/substrate.

This study aims at introducing the possibility of using brazing as a coating technology for surface protection. Although brazing is commonly regarded as a joining technique, the following research work presents a new and innovative solution for manufacturing functional coatings. In comparison with the previously mentioned techniques where a whole chain of complex equipment is usually required, for instance, for surface roughening or post processing, the presently described technology employs a single piece of equipment and entails fewer steps [18]. The increase in the use of fillers in aerospace, for machines exposed to heavy environments or microwave device, pushes the material development [19–21]. These realities, and the fact that this technique does not produce waste (compared, for instance, to thermal spraying where excess material is always left in the feeder), make the present technology cost-effective and extremely attractive for large-scale employment. Tape brazing is often performed by overlaying a flexible mat on top of a substrate prior to the coating at high temperatures. The flexible mat allows coatings on complex-shaped surfaces in a cost-effective way, as only a high-temperature vacuum furnace is needed. As a coating technique, it is expected to provide high cohesion and adhesion of the cladding to the substrate material [22,23]. High-temperature vacuum brazing is a viable alternative for improving the durability of industrial components exposed to high temperatures.

Experimental investigations were conducted in order to explore the microstructure, the susceptibility to high temperature corrosion, and the particle erosion behavior of vacuum brazed cobalt-based Amdry MM509B-C alloys deposited on an AISI 904L stainless-steel substrate. The feedstock materials (the powder and the organic binder) are adapted to the production of functional coatings aiming at increasing the component lifespan and at repairing worn surfaces (Co-based superalloys components). The manufacturing process of the tapes is accessible, economical, and environmentally friendly. Hot corrosion is an accelerated form of oxidation at temperatures higher than 600 °C in the presence of molten salts. Low-temperature hot corrosion (LTHC) is also known as Type II hot corrosion and occurs in the temperature range 600–750 °C. The mechanism involves a severe acidic fluxing of protective oxides (decomposition to the corresponding cations and O^{2-}). The localized corrosion attack is triggered by the formation of low melting point eutectics, consisting of sulphates of some elements from the base alloy and of alkali metal sulphates (ex. $CoSO_4/Na_2SO_4$) [24]. Depending on the kinetics of the corrosion reaction, two stages of hot corrosion can be reached, namely the initiation stage (initial slow stage) and the propagation stage (a much more severe stage of attack) [25]. The occurrence of LTHC attack shortens the time for which an alloy would be able to form protective oxide scales on the surface.

2. Materials and Methods

A cobalt-based powder with the commercial name Amdry MM509B-C from the company Oerlikon Metco, Langenfeld, Germany, was used as a brazing material. Its chemical composition contains boron as a melt-depressant and it is recommended to be used as

blend material for braze repairs, such as restoration of worn or damaged areas, crack repair, or restauration of surface flaws on aerospace and industrial gas turbine components [26].

The Amdry MM509B-C powder (particle size: –106 + 45 μm), having the chemical composition shown in Table 1, was mixed and bonded together with a water-based adhesive (Aleene's Tack-It Over and Over from Aleene's Duncan Enterprises Company, Fresno, CA, USA) in order to manufacture the coatings in form of flexible tapes. The tapes were manufactured by adding 6 wt.% adhesive to the brazing powder. Subsequently, by using a DRM 150 RE rolling mill from Durston, UK, the powder mixture was shaped into flexible tapes with a uniform thickness of 2 mm. The resulting tapes were then cut into the desired shape and size and positioned on 40 × 40 mm^2 AISI 904L stainless-steel (Fe, <0.02% C, 19–23% Cr, 23–28% Ni, 4–5% Mo, <2.0% Mn, <1.0% Si, <0.045% P, <0.035% S, 1.0–2.0% Cu) substrate material samples. The coating process was carried out at 3.5 10^{-2} Pa by vacuum brazing using a water cold-wall vertical controlled high-precision atmosphere furnace (HITERM 80–200, HITEC Materials, Karlsruhe, Germany), equipped with an oil sealed rotary and a turbomolecular pump. The iTools Engineering software served as user interface for the heat-treatment program development. Prior to the deposition, the stainless-steel substrate was cleaned with ethanol and ground with 1000 SiC paper to remove surface impurities.

Table 1. Chemical composition of Amdry MM509B-C powder.

Co wt. (%)	Cr wt. (%)	Ni wt. (%)	W wt. (%)	Ta wt. (%)	B wt. (%)	Ti wt. (%)	Zr wt. (%)	C wt. (%)
balance	22.4–24.25	9.0–11.0	6.5–7.5	3.0–4.0	2.0–3.0	0.15–0.30	0.30–0.60	0.55–0.65

The vacuum heat-treatment process parameters were established according to the recommendations of the Amdry brazing powder supplier and based on the literature reference [23]. The program used for experiments is illustrated in Figure 1.

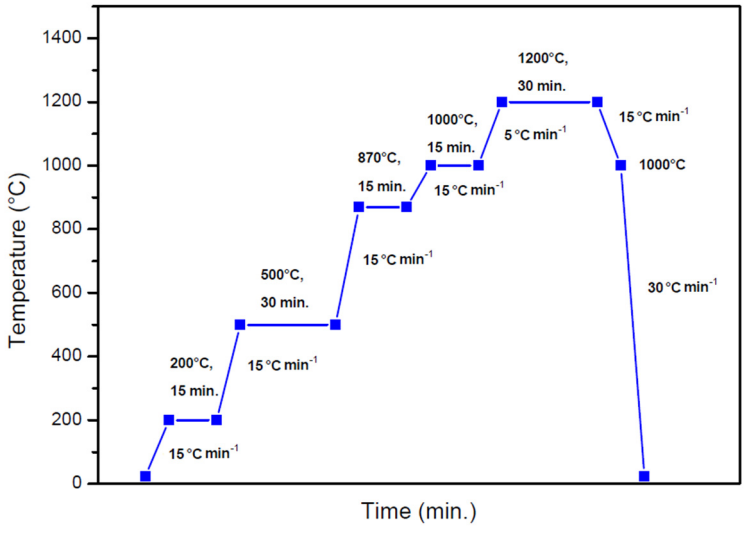

Figure 1. Experimental vacuum heattreatment brazing process parameters.

According to the powder supplier, the brazing temperature range should be set between 117 and 1260 °C. The coating deposition by vacuum brazing was accordingly performed at a maximum temperature of 1200 °C. The heating process was gradually performed with holding ramps (Figure 1) in order to provide enough time for the organic binder to decompose and for the powder alloy to melt and partially fill the gaps remaining from the decomposition of the organic binder.

The morphology and microstructure of the coatings were investigated by scanning electron microscopy (SEM: Quanta FEG 250, FEI, Hillsboro, OR, USA) equipped with

energy dispersive X-ray spectroscopy analysis (EDX with Apollo SSD: detector, EDAX Inc. Mahwah, NJ, USA) and by confocal laser scanning microscopy using a Keyence VK-X260K, Osaka, Japan. The SEM micrographs were acquired at a cathode voltage of 20 kV and a working distance of 11 mm.

The phase composition of the powder and brazed coating was identified at room temperature using a Philips X'Pert, Eindhoven, Netherlands diffraction equipment. The diffracted intensity was recorded at diffraction angle 2θ from 20 to 100°. The measurements were performed with a CuKα radiation source, in reflection mode, at 40 kV and 40 mA at a scan rate of 0.01° 2θ min^{-1}.

In order to evaluate the hot corrosion behavior, the coating and the substrate were sunk in two ceramic crucibles in a bath of salt mixture consisting of 25 wt.% NaCl+ 75 wt.% Na_2SO_4 and inserted in an oven at 750 °C for 100 h. The degree of corrosion attack was micrographically investigated in cross-section.

The erosion tests were carried out in accordance with ASTM G76. The samples (30 mm × 30 mm) were cleaned with acetone, dried, and weighed. The testing parameters were: Al_2O_3 erodent particles (d_{50} of 50μm), impingement angle 90°, nozzle to sample distance: 10 mm, dried and compressed air at 2 bar, particle mass flow rate: 7 g/min, testing time 20 min (divided in 4 periods of 5 min each). To ensure reproducibility, three samples of each batch were weighed at the beginning of the tests and every 5 min during testing.

The microhardness HV0.3 (load force 300 gf, dwell time 5 s) of the coatings was measured using a Zwick/Roell YHVμ-S, Ulm, Germany tester equipment.

3. Data analysis and Preliminary Results

3.1. Microstructural Analysis

Figure 2 shows the microstructure of the vacuum-brazed coating at different magnifications. The cross-section micrographs display a homogenous phase distribution and a small quantity of pores. No microcracks were identified. Despite the fact that the tapes were rolled to a thickness of 2 mm after the brazing process, the deposited material was densified, and the coating thickness was reduced to values ranging between 1.3 mm and 1.5 mm. Good adherence of the coating to the substrate is revealed by the interdiffusion line. The microstructure displayed in Figure 2a–c consists of a discontinuous and randomly oriented dendritic hypoeutectic microstructure, with primary dendrites of Co-based solid solution surrounded by interdendritic lamellar eutectic with Cr-, Co-, W- carbides, or even Laves phases. These regions appear in different greyscales, depending on the local chemical composition (Cr-rich or W-rich regions) [27–30].

By examining the chemical composition of the phases via EDX analysis (Figure 2d), it can be noticed that the eutectic regions marked with point 4 in Figure 2c are W-rich, whereas the eutectic regions marked with point 1 and 5 are Cr-rich (the difference of the grayscale is based on the different W or Ta content). Supplementary Ta-rich formations are marked with point 3 in Figure 2c and are randomly dispersed into the cobalt solid solution (point 2- Figure 2c). In this research, Ta-rich formations (although randomly dispersed) tend to lie in the proximity of the hard phases, and not near the substrate or the top of the coating, as suggested in the research reported by Mora-Garcia et al. [31]. The EDX analysis also reveals a certain degree of diffusion of the iron (Fe) into the deposited coating, which occurred during the vacuum brazing process [32]. In comparison with the findings of Xiong et al., who identified Cr as reacting at the interface, no such phenomena could be observed in the present research [33].

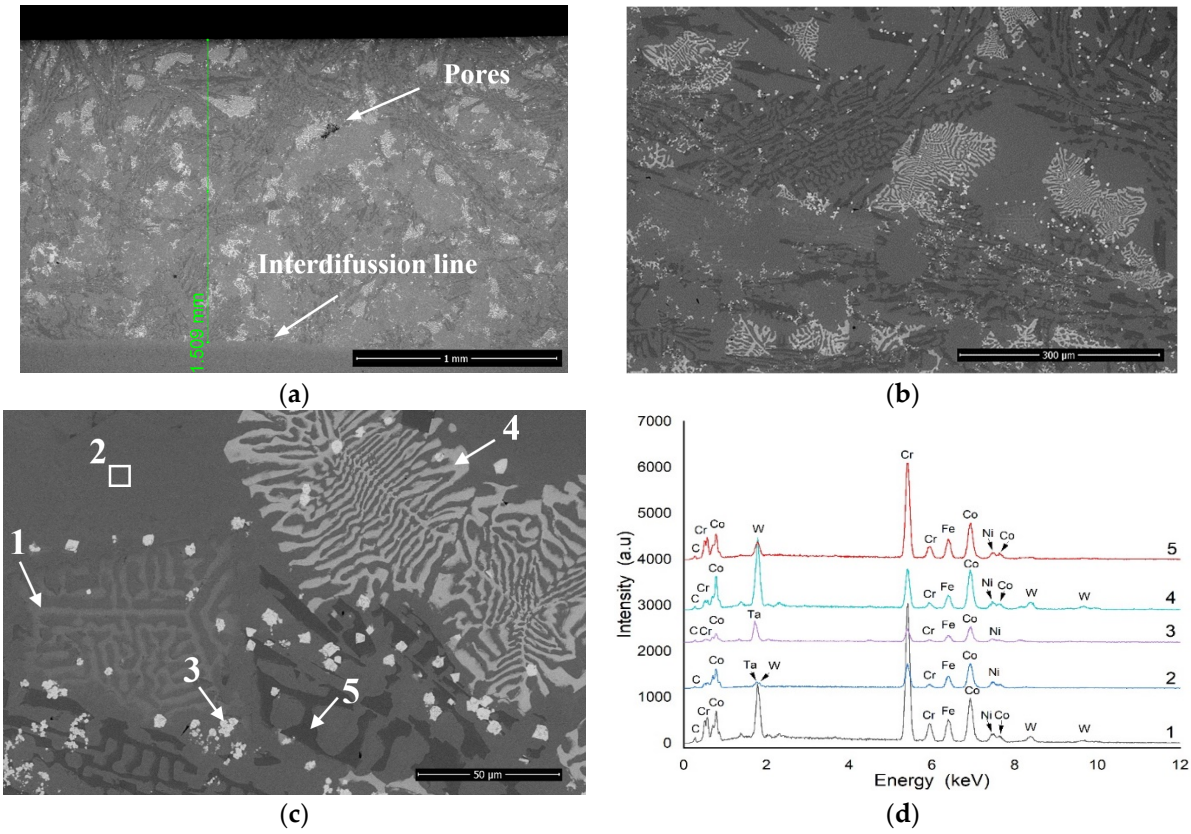

Figure 2. Cross-section back-scattered electron micrographs of the brazed coating (**a–c**); EDX-spectra (**d**).

3.2. XRD Diffraction Measurements

The XRD patterns of the powder and of the brazed coating are shown in Figure 3. In addition to Co, Ni, and Cr, the Amdry powder contains a small amount of chromium and cobalt carbides with lower carbon content ($Cr_{23}C_6$ and Co_3C). The obtained brazed coating contains, besides the Co-based solution, intermetallic phases (Laves type), a higher amount of Cr_7C_3 (higher carbon content), and cobalt-tungsten-carbides. The carbides formation was induced by the presence of carbon in the powder chemical composition and by the decomposition of the organic binder. In the W-Co-C ternary phase diagram [34], $M_{12}C$, formularized as CCo_2+xW_{4-x}, has a wide composition range from CCo_2W_4 (also found as Co_2W_4C) to Co_3W_3C [34]. In the present research, the high heat treatment temperature and the high W enabled the process of diffusion between the Co_3C and the W, producing the stoichiometrically stable CCo_2W_4 η-phase [35]. The formation of CCo_2W_4 is also supported by the existing literature, as this phase is referenced in the case of high-temperature processing, and only in the case with higher than 15% Co content. [36]. Cr_3Ni-based phases identified in the coating were also reported in recent literature, showing high hardness and excellent toughness in thermally sprayed Co-based materials [37,38]. Apart from enhancing the solidus point of the alloy, it has recently been reported that a high amount of Cr has a positive effect (in the case of brazing powders) on the shear strength and activation of the solution strengthening mechanism of the alloy [39].

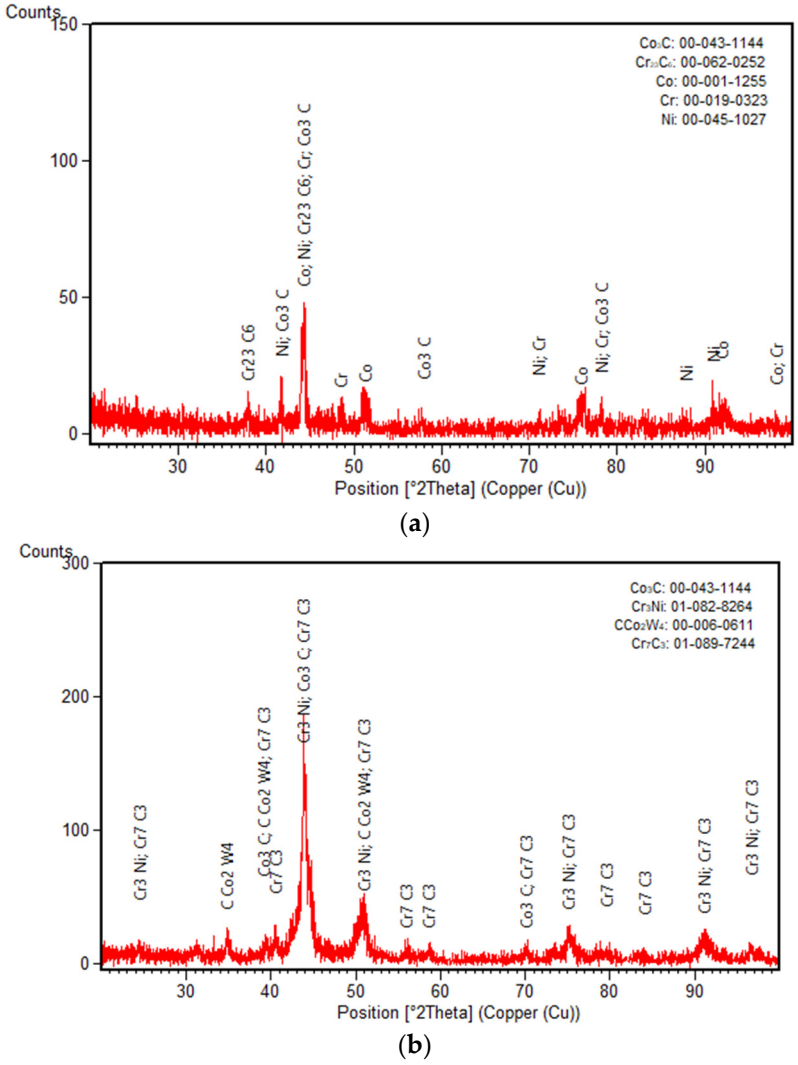

Figure 3. XRD pattern of the (**a**) cobalt-based Amdry MM509B-C powder and (**b**) brazed coating.

3.3. Hot Corrosion Behavior

The degree of corrosion attack of the brazed coating was investigated in comparison with that of the substrate material after 100 h of exposure to the hot salt mixture at 750 °C. A preferential localized material degradation based on acidic fluxing of the formed oxides occurred (marked with arrows—Figure 4a,b). The substrate material developed a thicker oxide scale on the surface, mainly consisting of Cr and Fe oxides (Figure 5a,b). The corrosion products contain S and Cl, besides the elements corresponding to the chemical composition of the stainless-steel.

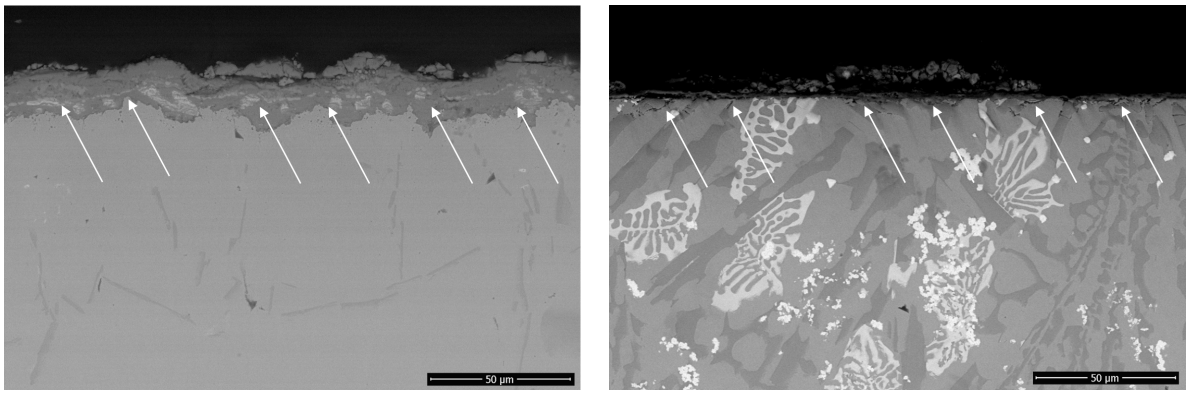

(**a**) (**b**)

Figure 4. Back-scattered electron micrograph (cross-section) of the substrate (**a**) and coating (**b**) exposed to LTHC.

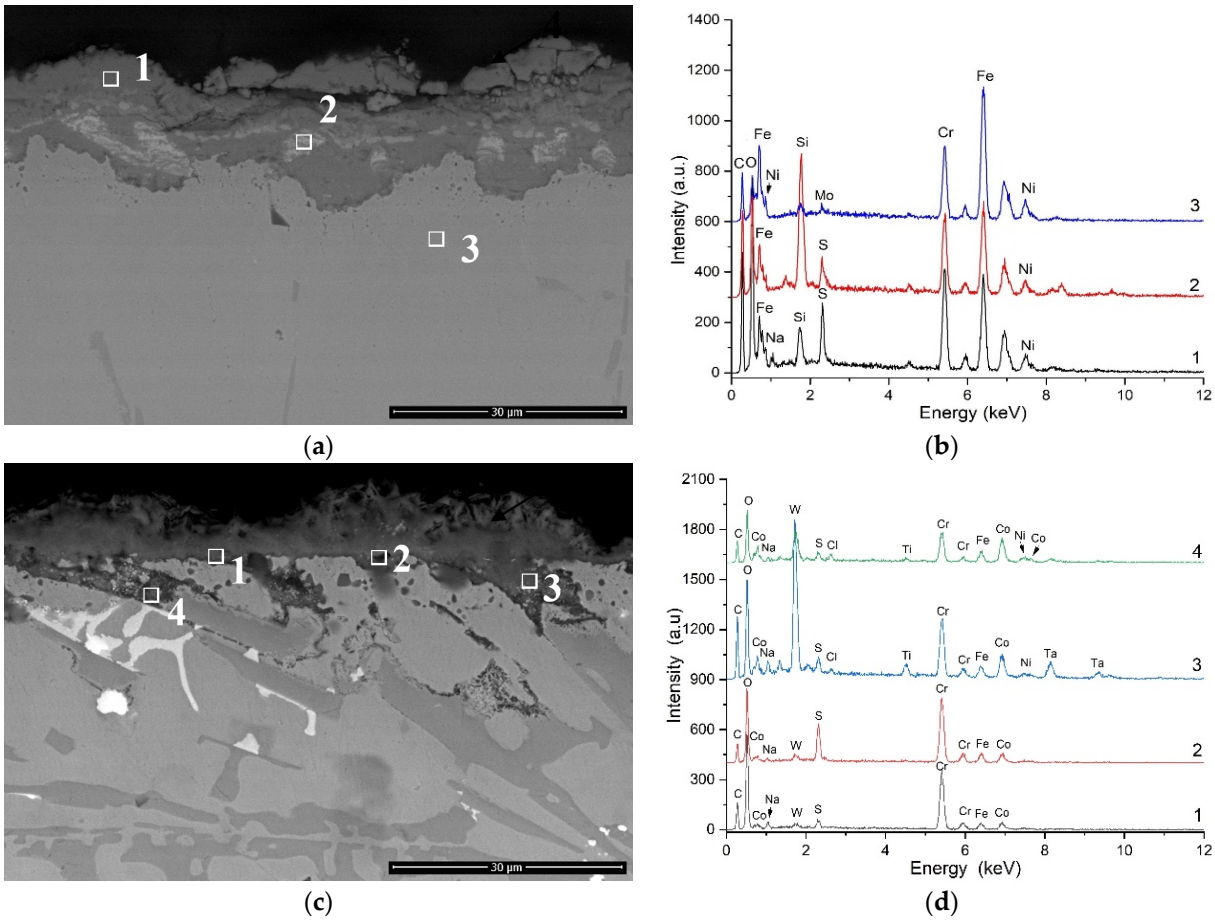

(**a**) (**b**)

(**c**) (**d**)

Figure 5. Cross-section back-scattered electron micrographs (higher magnification) of the corroded samples (**a**,**c**); EDX-spectra (**b**,**d**)

According to Figure 5c, the corrosion attack of the brazed coating is mainly concentrated in the regions of the eutectic from point 1, Figure 2c (with lower Cr-content), but also partially in the Co-based solid solution. The EDX chemical analysis (Figure 5b,d) indicates that the corrosion products formed on the sample surface consist mainly of Cr, O, and S, besides Fe and Ni. In addition to these elements, the oxidation products (in the case of the brazed coating) also comprise some easily diffused elements such as Co and Ta, which do not affect the surface state of the sample significantly [40]. The tendency of local corrosion

attack, especially in the region of grain boundaries, and a certain degree of spallation of the resulted hot corrosion products, mainly by stainless-steel substrate, are identified [41]. Literature reported that, due to the high thermal load in such experiments and the initial susceptibility of this area to hot corrosion, a phase segregation can occur [42,43]. The processing temperature for the coating manufacturing is crucial in order to ensure a good phase distribution and, most importantly, diffusion, so no segregation of the W-, Ta-, or Cr-rich phases occurs. The cooling process of the coating should be carefully performed, as internal stresses can also easily inflict damage to heterogeneous materials.

3.4. Solid Particle Erosion Resistance

The solid particles erosion test was performed three times for the coating and for the base material, respectively [44]. The variation of the erosion rate at an impact angle of 90° is shown in Figure 6. The damaged region of the sample surface generated during exposure to erosion was a circle of approximately 12 mm diameter. The stainless-steel substrate exhibited a lower erosion resistance compared to the one with the brazed coating under similar test conditions. After 20 min of testing, the mass loss for the coatings was about 4.8 ± 0.05 mg, compared with 8.4 ± 0.1 mg for the substrate.

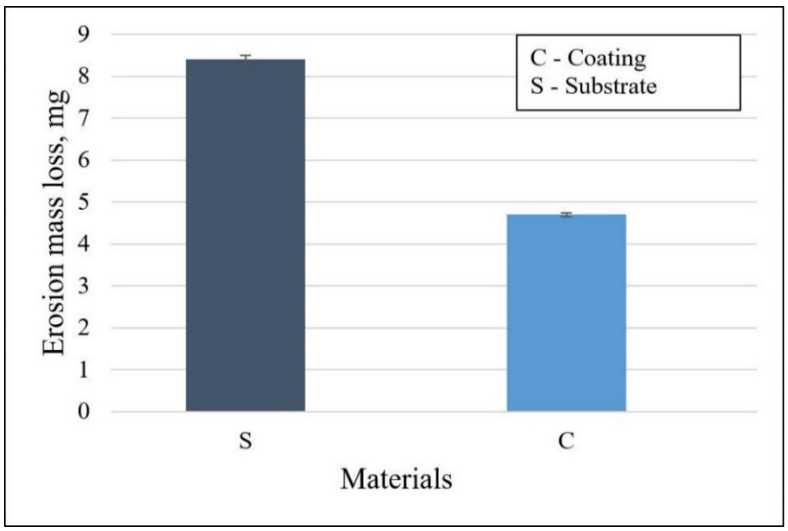

Figure 6. Histogram illustrating the material loss after the solid particle erosion test.

The Vickers microhardness values recorded on the cross section of samples are summarized in Figure 7. The microhardness values measured in the coating are higher than the ones recorded in the substrate, which corroborates a greater erosion resistance of the coating. The microhardness values of the coatings varied between 577 and 725 HV0.3, depending on the region where the microindentation was performed and on the material susceptibility to crack formation. Figure 8 illustrates the size of indentation path in a region with a higher number of hard phases, which is smaller than the one performed in the Co solid solution. It is known that carbides, silicides, or Laves phases are harder than Co-based solid solution [45]. Moreover, the absence of Palmqvist cracks that might have been formed from the corners of the Vickers indentation is an indicator of good fracture toughness. The crack propagations that could have appeared on the side of the indentation were effectively avoided due to the presence of the Cr_3Ni ductile intermetallic phase.

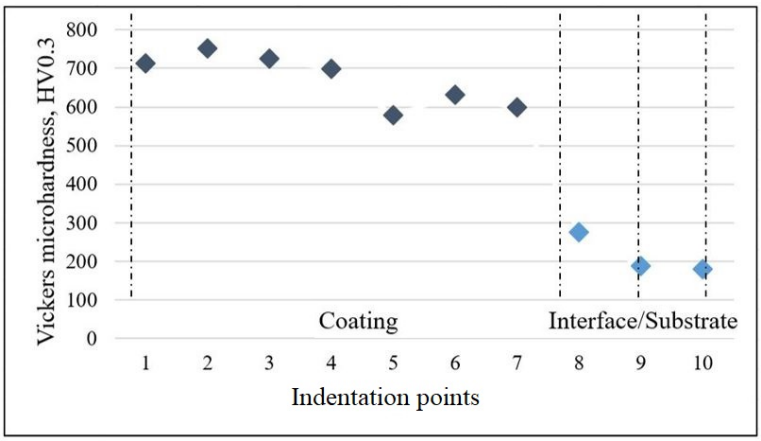

Figure 7. Microhardness values measured on the cross-section of the samples.

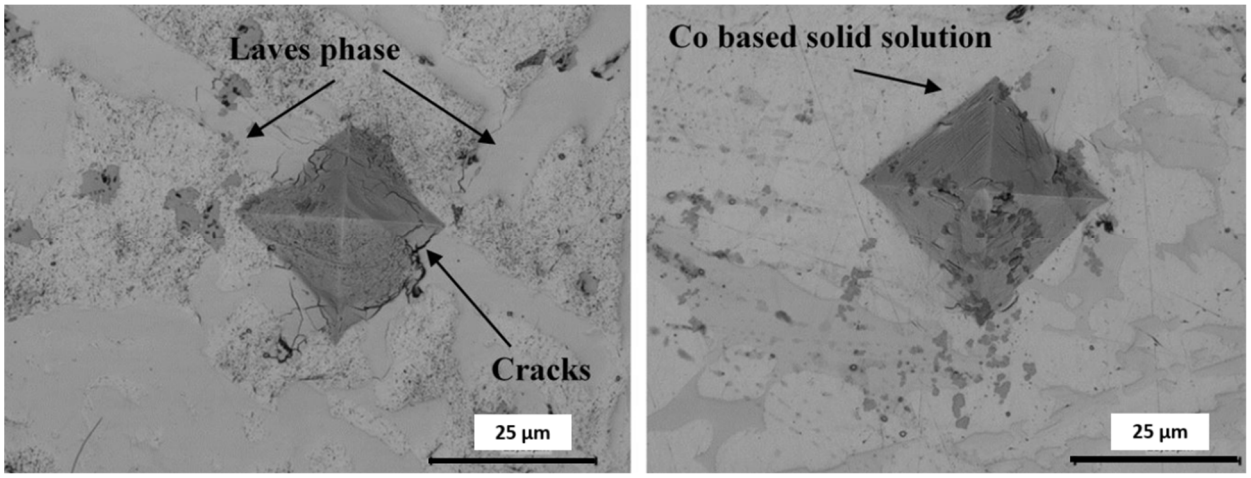

(**a**) (**b**)

Figure 8. Microscopic laser scanning micrographs of indentation mark of regions with (**a**) higher number of hard phases and (**b**) the Co solid solution on brazed coating.

The existing literature underlines that for 90°-impact angle solid particle erosion, a combination of hardness and toughness of coatings is more suitable than hardness alone, and a high resistance of cracks propagation is also a key factor for erosion resistance [46].

Nevertheless, this research unveils only a rough feeling about the fracture toughness and crack propagation phenomena of the coating. In-depth analyses entailing transmission electron microscopy, displacement, or loading–unloading curves could bring precise information regarding the elastic/inelastic behavior or failure points of the coating.

4. Conclusions

The microstructure, hot corrosion, and solid particles erosion resistance of Co-based alloys produced by vacuum brazing on the surface of a stainless-steel substrate were investigated. The results showed that vacuum brazing could be a cost-effective coating method for this type of chemical composition in order to produce surfaces with enhanced erosion and corrosion resistance.

The microstructure of the deposited brazed coatings showed a dense and homogenous dendritic microstructure with a CCo_2W_4 Laves phase and Cr_7C_3 carbides distributed in a Co-based matrix. Good adherence of the coating to the stainless-steel substrate was observed in the interface region. The EDX analysis highlighted that iron diffused into the coating during the brazing process. The hot corrosion behavior of the coatings revealed localized corrosion attacks, especially in the region of the chromium rich phases, mainly

forming chromium oxide-based corrosion products. The material degradation intensified with the increase in temperature. The formation of Laves phase and chromium and cobalt-based carbides in the coating microstructure (identified by diffractometry) exerted a positive impact on the hardness and erosive resistance, and thus improved the properties of the stainless-steel substrate.

Author Contributions: Conceptualization, I.-D.U.; methodology, I.-D.U., G.M., I.H. and N.K.; formal analysis, I.-D.U. and G.M.; investigation I.-D.U., I.H. and N.K., resources, I.-D.U., G.M. and A.T.C.; writing-original draft preparation, I.-D.U.; writing—review and editing I.-D.U., G.M., N.K. and A.T.C.; visualization I.-D.U., G.M., I.H., N.K. and A.T.C.; supervision, I.-D.U. and G.M. All authors have read and agreed to the published version of the manuscript.

Funding: The present work was partially funded through the DAAD (German Academic Exchange Service) program "Re-invitation Programme for Former Scholarship Holders, 2021" Ref. no. 91579356. This research was partially funded by a grant of the Romanian Ministry of Research, Innovation and Digitalization, project number PFE 26/30.12.2021, PERFORM-CDI@UPT100—The increasing of the performance of the Polytechnic University of Timișoara by strengthening the research, development and technological transfer capacity in the field of "Energy, Environment and Climate Change" at the beginning of the second century of its existence, within Program 1—Development of the national system of Research and Development, Subprogram 1.2—Institutional Performance—Institutional Development Projects—Excellence Funding Projects in RDI, PNCDI III.

Institutional Review Board Statement: Not applicable.

Informed Consent Statement: Not applicable.

Data Availability Statement: The data reported in this study are available from the authors upon request.

Acknowledgments: We acknowledge the support of eniz Kurumlu, in providing access to the Laboratory for Materials Science and Testing from Westfälische Hochschule Gelsenkirchen, Germany.

Conflicts of Interest: The authors declare no conflict of interest.

References

1. Singh, P.; Chauhan, S.S.; Singh, G.; Sharma, M.; Singh, V.P.; Vaish, R. Anticorrosion and Electromagnetic Interference Shielding Behavior of Candle Soot-Based Epoxy Coating. *J. Appl. Polym. Sci.* **2020**, *137*, 48678. [CrossRef]
2. Jiang, K. *Effects of Heat Treatment on Microstructure and Wear Resistance of Stainless Steels and Superalloys*; University of Ottawa: Ottawa, ON, Canada, 2013.
3. Bell, T. Surface Engineering of Austenitic Stainless Steel. *Surf. Eng.* **2002**, *18*, 415–422. [CrossRef]
4. Karafyllias, G.; Galloway, A.; Humphries, E. Erosion-Corrosion Assessment in Strong Acidic Conditions for a White Cast Iron and UNS S31600 Stainless Steel. *Wear* **2021**, *484–485*, 203665. [CrossRef]
5. Lo, K.H.; Shek, C.H.; Lai, J.K.L. Recent Developments in Stainless Steels. *Mater. Sci. Eng. R Rep.* **2009**, *65*, 39–104. [CrossRef]
6. Graf, K.; Tetzlaff, U.A.W.; de Souza, G.B.; Scheid, A. Effect of Dilution on the Microstructure and Properties of CoCrMoSi Alloy Coatings Processed on High-Carbon Substrate. *Mater. Res.* **2019**, *22*. [CrossRef]
7. Lin, W.C.; Chen, C. Characteristics of Thin Surface Layers of Cobalt-Based Alloys Deposited by Laser Cladding. *Surf. Coat. Technol.* **2006**, *200*, 4557–4563. [CrossRef]
8. Davis, J.R. *Nickel, Cobalt, and Their Alloys*; ASM International: Almere, The Netherlands, 2001; ISBN 0-87170-685-7.
9. Wen, J.; Che, H.; Cao, R.; Dong, H.; Ye, Y.; Zhang, H.; Brechtl, J.; Gao, Y.; Liaw, P.K. Evolution of the Mechanical Properties of a Cobalt-Based Alloy under Thermal Shocks. *Mater. Des.* **2020**, *188*, 108425. [CrossRef]
10. Liu, P.; Chen, D.; Wang, Q.; Xu, P.; Long, M.; Duan, H. Crystal Structure and Mechanical Properties of Nickel–Cobalt Alloys with Different Compositions: A First-Principles Study. *J. Phys. Chem. Solids* **2020**, *137*, 109194. [CrossRef]
11. Cinca, N.; López, E.; Dosta, S.; Guilemany, J.M. Study of Stellite-6 Deposition by Cold Gas Spraying. *Surf. Coat. Technol.* **2013**, *232*, 891–898. [CrossRef]
12. Yao, M.X.; Wu, J.B.C.; Yick, S.; Xie, Y.; Liu, R. High Temperature Wear and Corrosion Resistance of a Laves Phase Strengthened Co–Mo–Cr–Si Alloy. *Mater. Sci. Eng. A* **2006**, *435–436*, 78–83. [CrossRef]
13. Hu, H.X.; Guo, X.M.; Zheng, Y.G. Comparison of the Cavitation Erosion and Slurry Erosion Behavior of Cobalt-Based and Nickel-Based Coatings. *Wear* **2019**, *428–429*, 246–257. [CrossRef]
14. Kong, G.; Zhang, D.; Brown, P.D.; McCartney, D.G.; Harris, S.J. Microstructural Characterisation of High Velocity Oxyfuel Thermally Sprayed Stellite 6. *Mater. Sci. Technol.* **2003**, *19*, 1003–1011. [CrossRef]

15. Sidhu, B.S.; Puri, D.; Prakash, S. Mechanical and Metallurgical Properties of Plasma Sprayed and Laser Remelted Ni–20Cr and Stellite-6 Coatings. *J. Mater. Processing Technol.* **2005**, *159*, 347–355. [CrossRef]
16. Zhong, M.; Liu, W.; Yao, K.; Goussain, J.-C.; Mayer, C.; Becker, A. Microstructural Evolution in High Power Laser Cladding of Stellite 6+WC Layers. *Surf. Coat. Technol.* **2002**, *157*, 128–137. [CrossRef]
17. Cui, G.; Han, B.; Zhao, J.; Li, M. Comparative Study on Tribological Properties of the Sulfurizing Layers on Fe, Ni and Co Based Laser Cladding Coatings. *Tribol. Int.* **2019**, *134*, 36–49. [CrossRef]
18. Ahn, B. Recent Advances in Brazing Fillers for Joining of Dissimilar Materials. *Metals* **2021**, *11*, 1037. [CrossRef]
19. Jia, J.H.; Wang, Z.H.; Yao, D.F.; Tu, S.-T. Brazing Coupling Performance of Piezoelectric Waveguide Transducers for the Monitoring of High Temperature Components. *Sensors* **2021**, *21*, 94. [CrossRef]
20. Sharma, A.; Ahn, B. Brazeability, Microstructure, and Joint Characteristics of ZrO_2/Ti-6Al-4V Brazed by Ag-Cu-Ti Filler Reinforced with Cerium Oxide Nanoparticles. *Adv. Mater. Sci. Eng.* **2019**, *2019*, 8602632. [CrossRef]
21. Rybaulin, V.M.; Skorobatyuk, A.V.; Mikitas, A.V. Brazing of Absorbers of Planar Solar Heating Collectors Produced from Materials of the Cu–CuZn System. *Weld. Int.* **2016**, *30*, 142–149. [CrossRef]
22. Pascal, D.-T.; Kazamer, N.; Muntean, R.; Valean, P.-C.; Serban, V.-A. Electrochemical Corrosion Behavior of High Temperature Vacuum Brazed WC-Co-NiP Functional Composite Coatings. *IOP Conf. Ser. Mater. Sci. Eng.* **2018**, *416*, 012003. [CrossRef]
23. Pascal, D.-T. Development of High Temperature Vacuum Brazed WC-Co-NiP Functional Composite Coatings. Ph.D. Thesis, University Politehnica Timisoara, Timisoara, Romania, 2017.
24. Kalsi, S.S. Hot Corrosion and Its Mechanism: A Review. *Int. J. Emerg. Technol.* **2015**, *7*, 133–136.
25. Petit, F.; Meier, G.H. Oxidation and Hot Corrosion of Superalloys. *Supperalloys* **1984**, *85*, 651–687. [CrossRef]
26. Amdry MM509B-C Cobalt Braze Alloy Powder (Boron as Melt-Depressant). Available online: https://matmatch.com/materials/metc000058-amdry-mm509b-c-cobalt-braze-alloy-powder-boron-as-melt-depressant (accessed on 8 November 2021).
27. Bohatch, R.G.; Graf, K.; Scheid, A. Effect of Track Overlap on the Microstructure and Properties of the CoCrMoSi PTA Coatings. *Mater. Res.* **2015**, *18*, 553–562. [CrossRef]
28. Scheid, A.; D'Oliveira, A.S.C.M. Effect of Processing on Microstructure and Properties of CoCrMoSi Alloy. *Mater.Res.* **2013**, *16*, 1325–1330. [CrossRef]
29. Dong, Z.; Sergeev, D.; Dodge, M.F.; Fanicchia, F.; Müller, M.; Paul, S.; Dong, H. Microstructure and Thermal Analysis of Metastable Intermetallic Phases in High-Entropy Alloy $CoCrFeMo_{0.85}Ni$. *Materials* **2021**, *14*, 1073. [CrossRef]
30. Pilehrood, A.E.; Mashhuriazar, A.; Baghdadi, A.H.; Sajuri, Z.; Omidvar, H. Effect of Laser Metal Deposition Parameters on the Characteristics of Stellite 6 Deposited Layers on Precipitation-Hardened Stainless Steel. *Materials* **2021**, *14*, 5662. [CrossRef]
31. Mora-García, A.G.; Ruiz-Luna, H.; Mosbacher, M.; Popp, R.; Schulz, U.; Glatzel, U.; Muñoz-Saldaña, J. Microstructural Analysis of Ta-Containing NiCoCrAlY Bond Coats Deposited by HVOF on Different Ni-Based Superalloys. *Surf. Coat. Technol.* **2018**, *354*, 214–225. [CrossRef]
32. Rowe, A.P.; Bigelow, W.C.; Asgar, K. Effect of Tantalum Additions to a Cobalt-Chromium-Nickel Base Alloy. *J Dent Res* **1974**, *53*, 325–333. [CrossRef]
33. Xiong, H.-P.; Mao, W.; Xie, Y.-H.; Chen, B.; Guo, W.-L.; Li, X.-H.; Cheng, Y.-Y. Control of Interfacial Reactions and Strength of the SiC/SiC Joints Brazed with Newly-Developed Co-Based Brazing Alloy. *J. Mater. Res.* **2007**, *22*, 2727–2736. [CrossRef]
34. Lin, H.; Sun, J.; Li, C.; He, H.; Qin, L.; Li, Q. A Facile Route to Synthesize WC–Co Nanocomposite Powders and Properties of Sintered Bulk. *J. Alloy. Compd.* **2016**, *682*, 531–536. [CrossRef]
35. Guo, S.; Bao, R.; Yang, P.; Liu, L.; Yi, J. Morphology and Carbon Content of WC-6%Co Nanosized Composite Powders Prepared Using Glucose as Carbon Source. *Trans. Nonferrous Met. Soc. China* **2018**, *28*, 722–728. [CrossRef]
36. Bartha, L.; Kotsis, I.; Laczko, L.; Harmat, P. High Temperature Reactions of WC-Co Nanopowders in Various Atmospheres. In Proceedings of the 15 th International Plansee Seminar 2001, Reutte, Austria, 25–29 May 2001; Plansee Holding AG: Reutte, Austria, 2001; pp. 97–105.
37. Sharma, S.; Pandey, R.K.; Mishra, R.K.; Dixit, A. Improving Structure, Properties, and Abrasive Wear Resistance of the Thermally Sprayed Co-Based Coating by Means of La2O3 Addition. *Powder Metall. Met. Ceram.* **2016**, *54*, 672–678. [CrossRef]
38. Zhang, P.; Li, M.; Yu, Z. Microstructures Evolution and Micromechanics Features of Ni-Cr-Si Coatings Deposited on Copper by Laser Cladding. *Materials* **2018**, *11*, 875. [CrossRef] [PubMed]
39. Hosseini, E.; Amirjan, M.; Parvin, N. Preparation and Characterisation of Nickel-Based Brazing Powder: Cobalt and Chromium Addition Effects. *Powder Metall.* **2022**, 1–13. [CrossRef]
40. Chen, Z.; Geng, L.; Qu, W.; Wang, J.; Chen, M.; Li, S.; Wang, F. Characteristics and Hot Corrosion Resistance of Co-Deposition Layers with Different Activators and Al-Cr Ratios. *Corros. Sci.* **2022**, *202*, 110320. [CrossRef]
41. Liu, X.; Hu, K.; Zhang, S.; Xu, T.; Chen, L.; Byon, E.; Liu, D. Study of KCl-Induced Hot Corrosion Behavior of High Velocity Oxy-Fuel Sprayed NiCrAlY and NiCrBSi Coatings Deposited on 12CrMoV Boiler Steel at 700 °C. *Corros. Sci.* **2022**, *203*, 110351. [CrossRef]
42. Esmaeili, N.; Ojo, O.A. Analysis of Brazing Effect on Hot Corrosion Behavior of a Nickel-Based Aerospace Superalloy. *Metall. Mater. Trans. B* **2018**, *49*, 912–918. [CrossRef]
43. Fang, J.-H.; Ma, H.-W.; Xie, M.; Chen, Y.-T.; Yang, Y.-C.; Hu, J.-Q.; Wang, S. Effect of Joining Temperature and Bonding Time on Evolution of Interfacial Microstructure and Brazing Properties for 4J29/Ag–27Cu–4Ga/4J29 Brazed Joint. *Vacuum* **2019**, *167*, 459–470. [CrossRef]

44. Prasanna, N.D.; Siddaraju, C.; Shetty, G.; Ramesh, M.R.; Reddy, M. Studies on the Role of HVOF Coatings to Combat Erosion in Turbine Alloys. *Mater. Today Proc.* **2018**, *5*, 3130–3136. [CrossRef]
45. Sandhu, H.; Kumar, M. High-Termperature, Hardness and Wear Resistance of Cobalt-Based Tribaloy Alloys. *Int. J. Eng. Sci. Comput.* **2017**, *17*, 5411–5417.
46. Ma, A.; Liu, D.; Zhang, X.; Liu, D.; He, G.; Yin, X. Solid Particle Erosion Behavior and Failure Mechanism of TiZrN Coatings for Ti-6Al-4V Alloy. *Surf. Coat. Technol.* **2021**, *426*, 127701. [CrossRef]